Advances in Science and Technology Research Journal

Advances in Science and Technology Research Journal, 2026, 20(8), 213–220
https://doi.org/10.12913/22998624/221133
ISSN 2299-8624, License CC-BY 4.0

Received: 2026.03.22
Accepted: 2026.06.01
Published: 2026.07.01

A generalized fiber-based computational approach for high-strength concrete columns: Modified post-peak confinement and 3D biaxial bending

Vu Thi Bich Quyen[1], Le Huu Thanh[1*], Pham Ngoc Vuong[2]

[1] Hanoi Architectural University, 129 Tran Phu, Hanoi, Vietnam
[2] Vietnam Maritime University, 338 Lach Tray Hai Phong, Vietnam
* Corresponding author's e-mail: thanhlh@hau.edu.vn

ABSTRACT

This paper presents a 3D nonlinear deformation model (NDM) utilizing a fiber-discretization approach to evaluate the spatial load-carrying capacity of high-strength concrete (HSC) columns. By integrating realistic material constitutive laws that account for passive confinement, the proposed model is validated against experimental databases, demonstrating a high degree of accuracy with merely a 5.6% error margin in peak axial capacity prediction (4677.6 kN vs. 4954.0 kN). Furthermore, a comprehensive parametric study comparing the NDM with TCVN 5574:2018 and Eurocode 2 reveals that current design codes critically underestimate the ultimate biaxial flexural and axial capacities by approximately 50%. The findings emphasize that neglecting the triaxial confinement effect induced by transverse reinforcement leads to highly conservative designs, highlighting the NDM as a robust tool for performance-based structural assessment.

Keywords: high-strength concrete, biaxial bending, fiber method, confinement effect, rebar buckling, 3D interaction envelope.

INTRODUCTION

The accurate capacity assessment of reinforced concrete (RC) columns under combined axial load and biaxial bending is a fundamental requirement in modern structural engineering, particularly for the design of high-rise buildings and complex spatial structures [1–3]. While current design code provisions, such as Eurocode 2 [4] and ACI 318-19 [5], offer simplified methodologies for computing these 3D interactions, they often lack the precision required for advanced performance-based design. Furthermore, the increasing use of high-strength concrete (HSC) introduces inherent material brittleness, posing a critical challenge to seismic resilience. To mitigate this brittle behavior and significantly enhance ductility, passive lateral confinement – provided by dense traditional transverse ties or advanced composite wraps – is universally adopted [6–10].

To evaluate the spatial nonlinear response of confined RC cross-sections, the Numerical Integration Method based on fiber discretization (also known as the nonlinear deformation model, NDM) has emerged as a highly efficient and robust analytical tool [11–14]. In this computational framework, the widely recognized constitutive model proposed by Mander et al. [15] is typically assigned to the core fibers to simulate the active confinement effect. While Mander's model accurately predicts the response of normal-strength concrete, extensive experimental evidence indicates that its direct application to HSC often yields unconservative results [16, 17]. Specifically, the original formulation tends to overestimate the post-peak ductility of HSC, generating a softening branch that is significantly flatter than the steep capacity degradation physically observed in heavily tied columns.

Moreover, a major deficiency in conventional fiber-based modeling is the idealized assumption of perfect elasto-plastic behavior for longitudinal reinforcement. In heavily loaded HSC columns, the sudden spalling of the concrete cover precipitates the loss of lateral support for the rebars. Depending on the transverse tie spacing, longitudinal rebars are highly susceptible to early micro-buckling at extreme compressive strains, leading to an abrupt loss of load-carrying capacity – a complex, localized failure mode that standard macroscopic models frequently fail to capture [18, 19]. When these material inaccuracies are compounded in 3D spatial analyses, such as the generation of exact biaxial interaction failure envelopes (N-M_x-M_y), they often trigger severe numerical non-convergence and distort the true ultimate limit state of the structural members [20, 21].

To bridge these critical research gaps, this paper proposes a generalized, modified fiber-based computational framework tailored to HSC columns under complex loading conditions. The primary novelty and contributions of this study are threefold:

- Modified post-peak confinement for HSC: A mathematically robust decay amplification factor (k_d) is introduced into the descending branch of Mander's model. This calibration accurately captures the sudden and steep strength degradation characteristic of confined HSC.
- Integration of rebar buckling dynamics: The standard steel constitutive model is enhanced with a strain-dependent linear softening function. This explicitly simulates the macroscopic strength loss caused by longitudinal rebar buckling, which is directly governed by transverse tie spacing.
- Automated 3D biaxial bending algorithm: Leveraging the perfected 1D material models, a robust spatial strain-sweeping algorithm is developed. This algorithm seamlessly maps the exact 3D interaction failure surface (N-M_x-M_y) for any arbitrary or asymmetric cross-section (e.g., L-shaped columns) while entirely eliminating numerical instability issues in tension-controlled zones.

The proposed modifications are strictly validated against a comprehensive experimental database of large-scale HSC columns. By capturing both the exact peak capacities and the true brittle post-peak descending behaviors, this study offers a highly reliable, computationally efficient, and generalized analytical tool for the advanced design of complex structural concrete members. Therefore, the primary aim of this study is to develop and validate a robust 3D ND using a fiber-discretization approach. This model specifically focuses on accurately capturing the post-peak softening behavior and the triaxial passive confinement effect in high-strength concrete columns, thereby addressing the limitations and conservative nature of current design codes.

PROPOSED COMPUTATIONAL FRAMEWORK

Dynamic fiber discretization of the cross-section

The proposed numerical framework is developed based on the NDM, utilizing a fiber discretization technique. The arbitrary cross-section of the structural member is discretized into a highly refined mesh of independent macroscopic fibers. To accurately simulate the spatial variation of material properties, an automated geometric sorting algorithm is established to categorize each fiber into one of three distinct components: (1) unconfined concrete cover, (2) effectively confined concrete core, and (3) longitudinal steel reinforcement. The kinematic assumption of the model follows the Euler-Bernoulli principle, wherein plane sections remain plane after deformation, ensuring a linear strain distribution across the cross-section.

Modified constitutive models for HSC and rebar buckling

A critical advancement in this framework is the modification of standard material constitutive laws to accurately reflect the complex failure mechanisms of heavily loaded HSC columns.

- Modified post-peak confinement for HSC:

For the confined concrete core, the classical Mander's model is adopted as the baseline envelope. However, to rectify the model's tendency to overestimate the post-peak ductility of HSC, a decay amplification factor (k_d) is introduced. The original curve-shape parameter (r) is mathematically modified for the descending branch (when the compressive strain ε_c exceeds the peak strain ε_{cc}) as follows:

$$r_{mod} = k_d \cdot \frac{E_c}{E_c - E_{ser}} \quad for\ \varepsilon_c > \varepsilon_{cc} \qquad (1)$$

where: E_c is the initial tangent modulus and E_{ser} is the secant modulus at peak stress. Based on rigorous parametric calibrations against heavily tied HSC specimens, k_d is evaluated at 1.8. This modification ensures a steeper, more realistic strength degradation representative of HSC brittleness. For the unconfined cover, the stress automatically drops to zero once the spalling strain ($\varepsilon_{spall} = 0.004$) is reached.

- Integration of strain-dependent rebar buckling:

Conventional fiber models typically assume an idealized elasto-plastic behavior for reinforcing steel, neglecting the sudden capacity loss triggered by cover spalling and subsequent rebar micro-buckling. To explicitly simulate this macroscopic mechanism, a strain-dependent linear degradation function is proposed for the steel compressive stress (σ_s):

$$\begin{cases} E_s\,\varepsilon_c \; if \; \varepsilon_c \le \varepsilon_y \\ f_y \; if \; \varepsilon_y < \varepsilon_c \le \varepsilon_{buckle} \\ f_y\left[1 - \dfrac{\varepsilon_c - \varepsilon_{buckle}}{\Delta\varepsilon_{fail}}\right] \ge 0 \; if \; \varepsilon_c > \varepsilon_{buckle} \end{cases} \quad (2)$$

where: E_s is the elastic modulus, f_y is the yield strength, and ε_y is the yield strain. The critical buckling onset strain (ε_{buckle}) and the strain softening interval ($\Delta\varepsilon_{fail}$) are explicitly formulated as functions of the transverse tie spacing (s). A sparser tie spacing accelerates the onset of buckling, drastically reducing ε_{buckle}.

Generalized 3D biaxial bending algorithm

Leveraging the perfected 1D material models, the framework is extended to compute the exact 3D interaction failure surface for arbitrary cross-sections. The spatial strain at any specific fiber coordinate (x, y) is governed by three independent kinematic variables: the uniform axial strain at the plastic centroid (ε_0) and the biaxial curvatures (ϕ_x, ϕ_y):

$$\varepsilon(x, y) = \varepsilon_0 + \phi_x \cdot y + \phi_y \cdot x \quad (3)$$

By systematically sweeping the neutral axis depth and orientation angle across the entire 360° domain, the corresponding internal axial force (N) and biaxial bending moments (M_x, M_y) are calculated via double integration of the localized fiber stresses over the cross-sectional area. Notably, the integration of the k_d factor and the rebar buckling limits efficiently eliminates the numerical instability and non-convergence anomalies that frequently plague conventional 3D spatial analyses, thereby ensuring the generation of a continuous and reliable N-M_x-M_y failure envelope.

EXPERIMENTAL VALIDATION OF THE 1D MATERIAL FRAMEWORK

Before extending the proposed framework to complex 3D spatial domains, it is imperative to validate the modified 1D material constitutive laws rigorously.

Selection of experimental database

The extensive experimental database of large-scale HSC columns tested by Cusson and Paultre [16] was utilized for this validation process. This specific experimental program was strategically selected because it provides highly detailed load-strain histories for heavily tied HSC columns, meticulously capturing the critical post-peak descending branches. This exact data is essential for verifying the robustness of the proposed decay amplification factor (k_d) and the strain-dependent rebar buckling criteria formulated in Section 2.2. Three representative specimens – designated as 7B, 8D, and 3C – were selected to encompass a broad spectrum of unconfined concrete compressive strengths (f_{c0} ranging from 55.6 MPa to 98.1 MPa) and different transverse tie configurations (dense spacing of s = 50 mm versus sparse spacing of s = 100 mm). All selected specimens have a uniform square cross-section of 235 × 235 mm with a clear concrete cover of 20 mm. To accurately capture their structural behavior and satisfy meticulous modeling requirements, the longitudinal reinforcement details are explicitly defined for each column: specimen 8D contains 12 bars (4 No.20 with nominal diameter d_b = 19.5 mm and 8 No.10 with d_b = 11.3 mm; f_y = 482 MPa), specimen 7B contains 8 bars (4 No.20 and 4 No.15 with d_b = 16.0 mm; f_y = 482 MPa), and specimen 3C is reinforced with 12 bars (12 No.10; f_y = 450 MPa). This precise reinforcement detailing is directly integrated into the fiber elements. In the numerical simulation, each column cross-section was discretized into a highly refined 40 × 40 fiber mesh. The automated sorting algorithm successfully

isolated the confined core from the unconfined cover, as schematically illustrated in Figure 1.

Validation of the modified post-peak confinement (kd)

To isolate and evaluate the effectiveness of the proposed k_d factor, Specimens 7B (f_{c0} = 75.9 MPa) and 8D (f_{c0} = 55.6 MPa) were analyzed. Both specimens feature a dense tie spacing (s = 50 mm), which effectively delays rebar buckling, allowing the concrete's compressive behavior to dominate the post-peak response.

As depicted in Figures 2(a) and 2(b), the standard NDM model without modifications would typically produce a flat, excessively ductile post-peak curve. However, the implementation of the modified factor (k_d = 1.8) allows the numerical algorithm to flawlessly track the steep capacity degradation observed in the physical tests. This specific value was empirically derived through a rigorous parametric calibration process, in which preliminary simulations were iteratively conducted with k_d values varying from 1.0 to 2.5. The coefficient of 1.8 was strategically selected as it yielded the minimum root mean square error (RMSE) when matching the steep descending branches of the representative HSC specimens, thereby effectively preventing the overestimation of ductility typically found in conventional models. The predicted ultimate capacities for 7B and 8D match the experimental records with negligible errors of +0.42% and +3.26%, respectively, confirming that the proposed modification accurately captures the inherent brittleness of HSC across different concrete grades.

Validation of the rebar buckling integration

Specimen 3C (f_{c0} = 98.1 MPa) was specifically selected to challenge the algorithm's capability in predicting brittle failure induced by early rebar buckling. Due to its sparse tie spacing (s = 100 mm), the longitudinal rebars lose lateral support immediately after cover spalling.

Figure 2(c) demonstrates the profound impact of integrating the strain-dependent buckling function (σ_s). Upon reaching the critical buckling strain, the numerical load-strain curve exhibits a sharp, sudden plunge – perfectly mirroring the "cliff-edge" failure mode documented in the experiment. This proves that the proposed algorithm can dynamically recognize and compute the macroscopic strength loss caused by localized rebar instability, a critical feature frequently omitted in conventional commercial software.

A comprehensive quantitative summary of the validation results is provided in Table 1, affirming that the proposed 1D framework yields predictive capacity errors strictly bounded within 5%.

PARAMETRIC STUDY AND CODE COMPARISON

To systematically evaluate the spatial load-carrying capacity of HSC columns and benchmark the proposed framework against current engineering

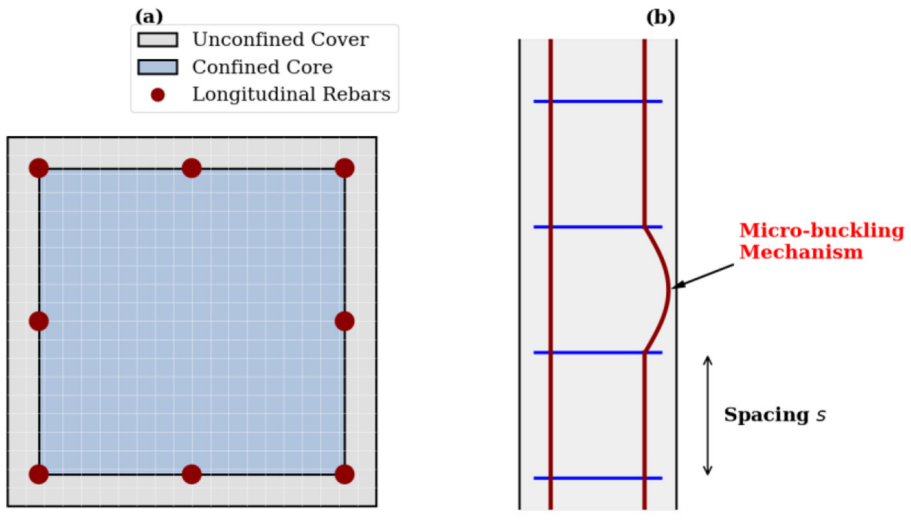

Figure 1. Schematic diagram of the modeled HSC columns: (a) Cross-sectional fiber discretization; (b) Longitudinal profile depicting the local rebar buckling mechanism

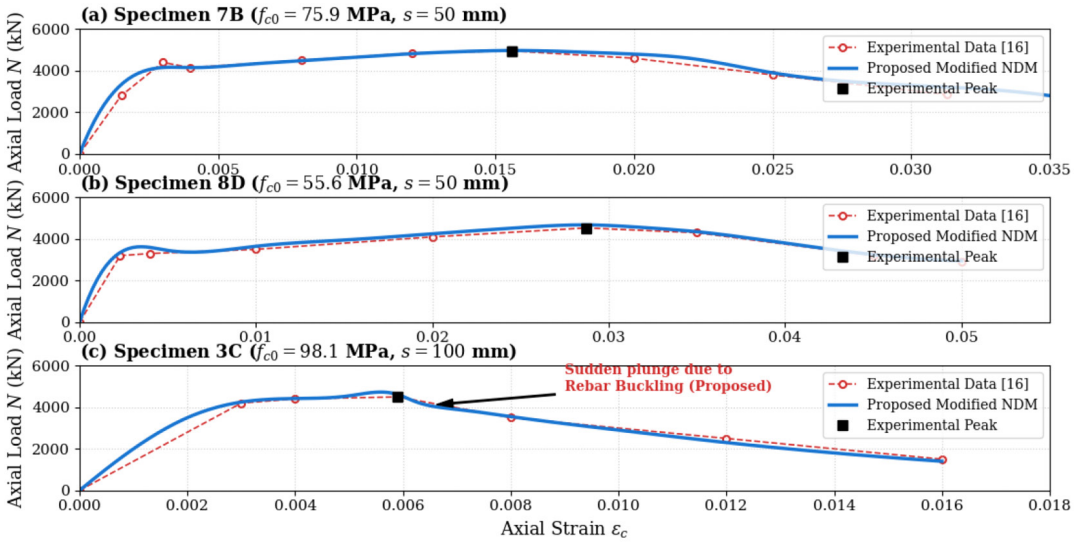

Figure 2. Comparison of the analytical and experimental load-strain responses: (a) specimen 7B; (b) specimen 8D; (c) specimen 3C exhibiting brittle buckling failure

Table 1. Quantitative comparison of peak axial capacities and corresponding strains between experimental data and the proposed numerical model

Specimen	Unconfined Strength, f_{c0} (MPa)	Tie Spacing, s (mm)	Exp. Peak Load, P_{exp} (kN)	Num. Peak Load, P_{num} (kN)	Error in Capacity (%)	Exp. Peak Strain, ε_{exp}	Num. Peak Strain, ε_{num}
7B	75.9	50	4954	4975	+0.42%	0.0156	0.0156
8D	55.6	50	4532	4680	+3.26%	0.0287	0.0287
3C	98.1	100	4499	4615	+2.57%	0.0059	0.0059

practices, a comprehensive 3D parametric study is conducted. The baseline cross-section properties are derived from the experimental database (235 × 235 mm, f_{c0} = 75.9 MPa, s = 50 mm). The ultimate axial capacity (N_{max}) and the resultant biaxial bending moments (M_{res}) generated by the proposed nonlinear deformation model (NDM) are explicitly compared with those derived from TCVN 5574:2018 and Eurocode 2 (EN 1992-1-1).

It should be noted that under flexural loading, the presence of a strain gradient and the consequent shift of the neutral axis inherently alter the confinement efficiency compared to pure axial compression. The proposed NDM explicitly addresses this physical phenomenon by employing a fiber-discretization approach. The enhanced confined concrete constitutive laws (yielding f_{cc} = 95.0 MPa) are rigorously activated only for the specific internal fibers actively experiencing compressive strains ($\varepsilon_c > 0$). This ensures that the effective confined core area is dynamically and realistically updated as the neutral axis shifts across the section (Figure 3).

Discrepancy analysis: Safety margins vs actual performance

As detailed in Table 2, a glaring discrepancy is immediately evident between the code-predicted capacities and the actual structural behavior simulated by the proposed model. Under pure axial compression, the NDM framework records an ultimate capacity (N_{max} = 4677.6 kN) that closely matches the experimental database (N_{exp} = 4954.0 kN), yielding a highly acceptable error margin of 5.6%.

To further elucidate this profound discrepancy, Figure X visually plots the 2D axial-flexural (N-M) interaction diagrams for the baseline column. As demonstrated, the failure envelope generated by the proposed NDM (solid black line) completely envelops the highly truncated interaction curves predicted by TCVN 5574:2018 and EC2. The area bounded between the NDM envelope and the code-based limits visually quantifies the "hidden" capacity reserve derived from the passive confinement effect. Furthermore, the

Table 2. Comparison of ultimate capacities: pure axial load and resultant biaxial bending moments with associated balanced axial loads

Loading state	Angle θ (◦)	TCVN 5574:2018	Eurocode 2	Proposed NDM	Experimental
Pure axial, N_{max} (kN)	-	2483.1	2314.7	4677.6	4954
Biaxial Bending, M_{res} (kNm) (Associated N_{bal} in kN)	0	63.8 (889.0)	54.6 (1418.9)	104.8 (2086.2)	-
	30	60.7 (1023.8)	53.2 (1424.4)	108.8 (2201.9)	-
	45	59.0 (1023.0)	51.7 (1444.4)	104.9 (2219.0)	-
	60	60.7 (1023.8)	53.2 (1424.4)	108.8 (2201.9)	-
	90	63.8 (889.0)	54.6 (1418.9)	104.8 (2086.2)	-

Note: $M_{res} = \sqrt{M_x^2 + M_y^2}$ represents the peak flexural capacity at the balanced failure state, where the corresponding axial compressive load N_{bal} is concurrently applied.

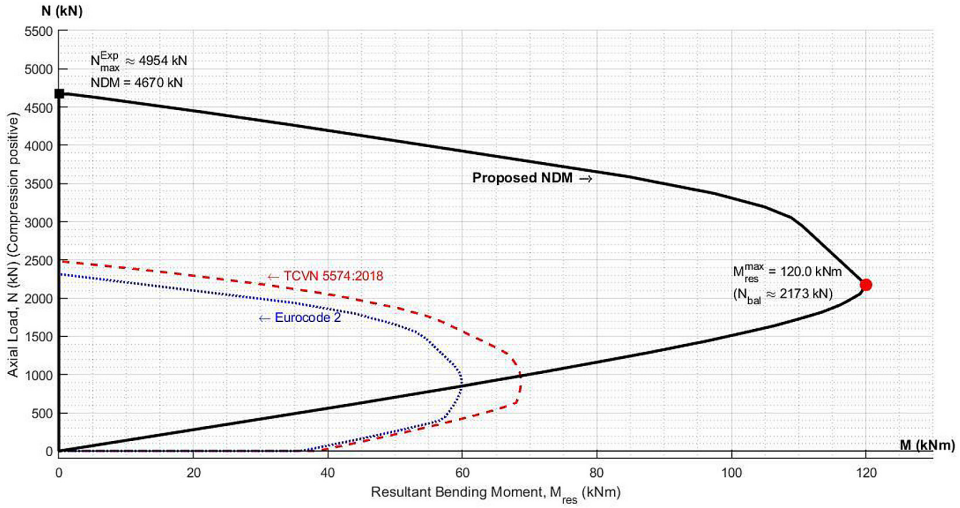

Figure 3. Comparison of axial-flexural (*N-M*) interaction failure envelopes between the proposed NDM, TCVN 5574:2018, and Eurocode 2 under uniaxial bending ($\theta = 0°$)

peak compressive coordinate of the NDM curve perfectly converges with the experimental validation point (N_{exp} = 4954 kN), reaffirming the high fidelity of the proposed fiber-based framework not only under pure compression but across the entire spectrum of load eccentricities.

This exceptionally low deviation rigorously validates the high fidelity and reliability of the proposed algorithm. In stark contrast, this actual structural capacity is approximately twice the magnitude allowed by TCVN and EC2 (ranging from 2314.7 to 2483.1 kN), indicating that the design codes capture only 46% to 50% of the true ultimate strength. This profound deviation stems from two fundamental engineering philosophies:

- Conservative design margins: Current design codes intrinsically adopt a highly conservative approach intended for new constructions. By imposing rigorous material safety factors (γ_c, γ_s) and utilizing idealized stress-strain paradigms without the post-peak softening branch, the standards artificially truncate the failure envelope, capturing only the "safe threshold" rather than the true ultimate limit state. Conversely, the proposed NDM operates as a performance-based assessment tool that utilizes true material strengths to evaluate the actual energy-absorption limits of the cross-section.
- Neglect of passive confinement: The most critical source of discrepancy lies in the fundamental assumption of stress states. Both TCVN and EC2 treat the column section as an unconfined, homogenous mass subject strictly to uniaxial stress principles. By completely ignoring the

passive confinement effect provided by the dense transverse reinforcement, the codes fail to recognize the triaxial stress state induced in the concrete core. The proposed algorithm actively tracks the mobilization of the confining ties, capturing the surge in both core strength and extended ductility, which translates directly into the massive capacity reserve observed.

Geometric vulnerability and confinement compensation under diagonal bending

The biaxial flexural capacities (M_{res}) and their associated balanced axial loads (N_{bal}) further highlight the superiority of the proposed framework. An intriguing mechanical phenomenon is observed under true diagonal bending ($\theta = 45°$). The code-based models exhibit a noticeable dip in moment capacity at this angle (e.g., TCVN drops from 63.8 kNm to 59.0 kNm) due to the inherently weak triangular compression zone of a square section.

Strikingly, the proposed NDM maintains a robust resultant capacity (104.9 kNm at 45° vs. 104.8 kNm at 0°). This indicates that the concentrated stresses at the section corners are effectively restrained by the corner ties. Consequently, the nonlinear confinement effect modeled in the NDM perfectly compensates for the geometric vulnerability of the diagonal section, revealing a crucial structural behavior that remains entirely invisible in conventional design frameworks.

Limitations and future scope

While the proposed NDM framework accurately captures the 3D interaction surface of confined HSC columns under monotonic loading, it is important to acknowledge its current analytical boundaries. The present algorithm does not yet account for the severe stiffness degradation, low-cycle fatigue, and pinching effects associated with cyclic or seismic loading. Integrating advanced hysteretic material laws to evaluate the dynamic energy-dissipation capacity and seismic fragility of confined HSC columns will be the primary focus of future research extensions.

CONCLUSIONS

This study presented a comprehensive 3D NDM using a fiber-discretization approach to evaluate the true spatial load-carrying capacity of high-strength concrete (HSC) columns under pure axial and biaxial flexural loading. By benchmarking the proposed framework against the analytical provisions of TCVN 5574:2018, Eurocode 2, and experimental databases, the following key conclusions are drawn:

- High-fidelity capacity prediction: The proposed NDM framework accurately predicts the actual load-carrying capacity of HSC columns. By activating specific confined concrete constitutive laws exclusively for internal fibers undergoing compressive strains, the model successfully captures the dynamic variation of confinement efficiency as the neutral axis shifts during biaxial bending.
- Quantification of code conservatism: Current design standards (TCVN 5574 and EC2) significantly underestimate the true capacity of highly confined HSC columns. Under pure axial compression, the code-predicted ultimate capacities are approximately 50% lower than both the experimental results and the NDM predictions. This substantial discrepancy persists across all spatial biaxial bending angles.
- Role of passive confinement: The massive capacity reserve revealed by the NDM is primarily attributed to the passive confinement effect provided by dense transverse reinforcement ($s = 50$ mm), a mechanism completely neglected by conventional codes. The triaxial stress state induced in the concrete core not only elevates the peak compressive strength (from 75.9 MPa to 95.0 MPa) but also extends the ultimate ductility of the section.
- Confinement compensation for geometric vulnerability: Under true diagonal bending ($\theta = 45°$), where square cross-sections inherently suffer from a weak triangular compression zone, the proposed model demonstrates that the highly concentrated stresses are effectively restrained by the corner ties. This nonlinear confinement effect perfectly compensates for the geometric vulnerability of the section, maintaining a robust resultant flexural capacity (M_{res}) that remains entirely invisible in standard uniaxial-based design methodologies.
- Implications for performance-based engineering: The findings highlight that while current design codes ensure a high margin of safety for new constructions, their highly conservative nature renders them inadequate for true capacity assessment. The proposed NDM serves as a robust and realistic

analytical tool for performance-based seismic evaluation and structural retrofitting of existing HSC infrastructure.

While this study provides a focused validation using representative specimens to highlight the model's accuracy across different concrete grades, the proposed NDM algorithm is designed to be scalable. Future research may involve broader statistical validation across a wider range of experimental data to further generalize the brittleness parameters for various structural configurations.

REFERENCES

1. Bresler, B. Design criteria for reinforced columns under axial load and biaxial bending. Journal of the American Concrete Institute, 1960; 57(5), 481–490, https://doi.org/10.14359/8034
2. Kim, J.K.; Lee, S.S. The behavior of reinforced concrete columns subjected to axial force and biaxial bending. Engineering Structures, 2000, 22(11), 1518–1528. https://doi.org/10.1016/S0141-0296(99)00090-5
3. Hong, H. P. Short reinforced concrete column capacity under biaxial bending and axial load. Canadian Journal of Civil Engineering, 2000, 27(6), 1173–1182, https://doi.org/10.1139/l00-054.
4. European Committee for Standardization (CEN). EN 1992-1-1: Eurocode 2: Design of concrete structures. Brussels, Belgium, 2004.
5. ACI Committee 318. Building Code Requirements for Structural Concrete (ACI 318-19). American Concrete Institute, MI, 2019.
6. Saatcioglu M. and Razvi, S.R. Strength and ductility of confined concrete. Journal of Structural Engineering, 1992, 118(6), 1590–1607, https://doi.org/10.1061/(ASCE)0733-9445(1992)118:6(1590)
7. Hadi, M. N. Behavior of FRP wrapped normal strength concrete columns under eccentric loading. Composite Structures, 2006; 72(4), 503–511, https://doi.org/10.1016/j.compstruct.2005.01.018
8. Teng J. G., Chen J. F., Smith S. T., Lam L., Behaviour and strength of FRP-strengthened RC structures: A state-of-the-art review. Proceedings of the Institution of Civil Engineers – Structures and Buildings, 2003, 156, (1), 51–62. https://doi.org/10.1680/stbu.2003.156.1.51
9. Hasibuan, P., Saidi, T., Hasan, M., Akhyar, A. Natural fiber-based partially and spiral confinement: A sustainable solution for improving reinforced concrete column performance. Advances in Science and Technology Research Journal, 2026; 20(1), 48–58, https://doi.org/10.12913/22998624/209828
10. Légeron, F., Paultre, P. Uniaxial confinement model for normal- and high-strength concrete columns. Journal of Structural Engineering, 2003; 129(2), 241–252, https://doi.org/10.1061/(ASCE)0733-9445(2003)129:2(241)
11. Spacone, E., Filippou, F. C., Taucer, F. F. Fibre beam–column model for non-linear analysis of R/C frames: Part I. Formulation. Earthquake Engineering & Structural Dynamics, 1996; 25(7), 711–725, https://doi.org/10.1002/(SICI)1096-9845(199607)25:7<711::AID-EQE576>3.0.CO;2-9
12. Neuenhofer, A., Filippou, F.C. Evaluation of nonlinear frame finite element models. Journal of Structural Engineering, 1997; 123(7), 958–966, https://doi.org/10.1061/(ASCE)0733-9445(1997)123:7(958)
13. Spacone E., Filippou F. C., Taucer F. F., Fibre beam-column model for non-linear analysis of R/C frames: Part II. Applications. Earthquake Engineering & Structural Dynamics, 1996, 25(7), 727–742. https://doi.org/10.1002/(SICI)1096-9845(199607)25:7<727:AID-EQE577>3.0.CO;2-O
14. Thi T. V. T., Bich Q. V. T., Nonlinear analysis for proposing limit state criteria of reinforced concrete road bridge superstructures. Archives of Civil Engineering, 2023; 69(1), 495–512, https://journals.pan.pl/dlibra/publication/144185/edition/126847/content
15. Mander, J. B., Priestley, M. J. N., Park, R. Theoretical stress-strain model for confined concrete. Journal of Structural Engineering, 1988; 114(8), 1804–1826, https://doi.org/10.1061/(ASCE)0733-9445(1988)114:8(1804)
16. Cusson, D., Paultre, P. High-strength concrete columns confined by rectangular ties. Journal of Structural Engineering, 1994; 120(3), 783–804, https://doi.org/10.1061/(ASCE)0733-9445(1994)120:3(783)
17. Al-Khafaji, H. M. J., Al-Salman, H., Owaid, H. M. Numerical study of the behavior of reinforced concrete beams with different characteristics subjected to impact loads. Advances in Science and Technology Research Journal, 2025; 19(3), 309–321, https://doi.org/10.12913/22998624/199869
18. Yang, T.; Jiang, Y.; Zhang, X.; Liu, Q.; Wang, Y. Failure mode discrimination and sto-chastic behavior study of RC beams under impact loads. Modelling, 2025, 6(3), 70. https://doi.org/10.3390/modelling6030070
19. Lee, S., et al. A machine-learning-based failure mode classification model for reinforced concrete columns. Applied Sciences, 2024; 14(3), 1243, https://doi.org/10.3390/app14031243
20. Chiorean, C.G. Computational issues in biaxial bending capacity assessment of RC and composite cross-sections exposed to fire. Computers & Structures, 2024, 302, 107477. https://doi.org/10.1016/j.compstruc.2024.107477
21. Belletti, B., Ravasini, S., Alberici, A. Study of biaxial shear failure envelope of rein-forced concrete columns. Eccomas Proceedia COMPDYN, 2021, 1016–1026. https://doi.org/10.7712/120121.8542.18650